Wave functions associated with time-dependent, complex-scaled Hamiltonians evaluated on a complex time grid

Jakob Bengtsson,[1] Eva Lindroth,[1] and Sølve Selstø[2]
[1]*Department of Physics Stockholm University, AlbaNova University Center, SE-106 91 Stockholm, Sweden*
[2]*Faculty of Technology, Art and Design, Oslo and Akershus University College of Applied Sciences, NO-0130 Oslo, Norway*
(Received 7 December 2011; published 30 January 2012)

We solve the time-dependent Schrödinger equation with the method of uniform complex scaling and investigate the possibility to evaluate the solution on a complex time grid. With this approach it is possible to calculate properties that relate directly to the continuum part of the complex scaled wave function, such as the photoelectron spectrum after photoabsorption.

DOI: 10.1103/PhysRevA.85.013419 PACS number(s): 32.80.Rm, 31.15.−p

I. INTRODUCTION

The method of uniform complex scaling [1–4] (also known as complex rotation), which is based on a continuation of the radial variable into the complex-valued plane [$r \to r\exp(i\theta)$], is a widely used technique. It is, for example, particularly well suited for identification and characterization of multiply excited electronic states coupled by Auger transitions to the "ordinary" continuum of states and has, for this purpose, been combined with a range of computational methods, see, e.g., Refs. [5–16]. For large-enough scaling angles, θ, the wave function describing such a *resonance* state becomes exponentially damped in the asymptotic region of r. The L^2-normalizable state hereby produced can then, just as any bound eigenstate, be obtained as the eigenstate of the now "scaled" Hamiltonian, $H^\theta(r) \equiv H[r\exp(i\theta)]$, which is non-Hermitian by construction. The eigenvalues of H^θ are generally complex and for a resonance state, the real and imaginary components are associated with energy position and width, respectively. The same information cannot be obtained in such a direct way from the energy spectrum of any corresponding Hermitian Hamiltonian. With a Hermitian formulation it is instead a local accumulation of pseudocontinuum states in the real energy domain that reveals the existence of a resonance.

Atoms exposed to electromagnetic fields can also be treated most favorably with the complex scaling method. The decay (or ionization) rate of an initially prepared system is, for instance, given directly by the spectrum of the (time-independent) scaled Hamiltonian, similarly to the situation for the field-free case. The considered atom might be exposed to either a static field [17–19] or, with the construction of the Floquet-Hamiltonian [20], to a time-periodic one [17,21,22]. If the electromagnetic field is in the form of a sufficiently short pulse, it is eventually necessary to solve the time-dependent Schrödinger equation through explicit time propagation. Still uniform complex scaling has proven to be a fruitful method, at least as long as the physical information is retrieved from the bound part of the wave function. A convincing demonstration of this was made by Scrinzi and Piraux [23] for two electron atoms exposed to short laser pulses. Their work also underlined an additional (apart from the ability to account for resonances) desirable property of complex rotation; the unstructured continuum can be represented by surprisingly few states. This property was also discussed in some detail in Ref. [24] and exploited in order to solve the time-dependent Dirac equation in Ref. [25].

In the time-dependent studies just mentioned [23,25] the information that was obtained from the wave function was primarily coming from the bound part, e.g., the ground state survival probability after exposure to the pulse. It is less evident if, and, in that case, how, information about the continuum part, giving, for example, the photoelectron spectrum, of the time propagated wave function can be accessed. One possibility could be to use some kind of back-transformation, see, e.g., Refs. [24,26,27]. Although such methods have been shown to be applicable on selected model examples, they are generally not feasible for calculations of realistic situations. Here we propose an alternative method to retrieve the information from the complex rotated and time-propagated wave function. The key ingredient in the method is that the time propagation is made with a complex time coordinate. In Sec. II we briefly review some properties of uniform complex scaling, with particular emphasis on the time-dependent situation, Sec. II C. In Sec. III the propagation on a complex time-grid is discussed and some numerical results are also shown.

II. COMPLEX SCALING

A. General remarks

With uniform complex scaling, the radial variable is transformed as

$$r \to re^{i\theta}, \tag{1}$$

and the Hamiltonian is transformed accordingly, i.e.,

$$H^\theta(\mathbf{r},t) \equiv H(\mathbf{r}e^{i\theta},t). \tag{2}$$

The scaling angle is in the range $0 < \theta < \pi/4$. The eigenvalues of the scaled Hamiltonian are generally complex, and the imaginary parts are connected to decay rates. It is illustrative to consider how the eigenstates of this Hamiltonian will be found in practice: In a typical numerical calculation a finite set of L^2 functions will span a domain to which the Hamiltonian is eventually restricted. Approximate eigenstates of the Hamiltonian are then found by diagonalization of its matrix representation in this finite space. As a consequence, we find a finite number of eigenvalues; one subset with real energies corresponding to bound states and a second subset forming a so-called *pseudocontinuum* with positive energies

rotated approximately as $E \to E\exp(-i2\theta)$ and, depending on the particular physical system, a set of complex energy eigenvalues that are independent of the scaling angle, i.e., corresponding to resonances. Only the first subset of these eigenvalues, i.e., corresponding to bound states and with real energies, will be identical to the eigenvalues of the corresponding unrotated Hamiltonian.

Turning to the eigenvectors, we find also here a distinct difference compared to the unrotated case. For a Hermitian matrix the left, $\mathbf{L}$, eigenvector with a certain eigenvalue is the complex conjugated transpose of the right, $\mathbf{R}$, eigenvector with the same eigenvalue, and, thus, we have the familiar form of the inner product. For a complex rotated (originally Hermitian) matrix the left eigenvector of the matrix after rotation with θ is, instead, the complex conjugated transpose of the right eigenvectors of the matrix after rotation with $-\theta$, see, e.g., the discussions in Refs. [24,28], i.e.,

$$\mathbf{L}^{\theta} = (\mathbf{R}^{-\theta})^{\dagger}. \tag{3}$$

Note, thus, that while $\mathbf{L}^{\theta}$ is the left eigenvector of H^{θ} with eigenvalue E^{θ}, $\mathbf{R}^{-\theta}$ is the right eigenvector of $H^{-\theta}$ with eigenvalue $E^{-\theta} = (E^{\theta})^{*}$. The special case of complex rotation of an originally real symmetric matrix will give a complex symmetric matrix where $\mathbf{L}^{\theta} = (\mathbf{R}^{\theta})^{T}$. When complex rotation is employed to time-independent problems the matrix is usually complex symmetric and most authors calculate the inner products with the left eigenvector being just the transpose of the right eigenvector without much discussion. As will be evident below, the distinction between the two eigenvectors becomes much more important for time-dependent calculations. However, before entering the discussion on the time-dependent case we will, as an illustration, discuss the photoelectron spectrum. It is an example of an important physical observable which has to be derived from the continuum part of the wave function. How can we calculate it from a complex rotated wave function?

B. The photoelectron spectrum

The photoabsorption cross section in the weak-field limit is conveniently calculated with complex rotation as [29]

$$\sigma(\omega) = \frac{e^2}{4\pi\epsilon_0}\frac{4\pi}{3}\frac{\omega}{c} \times \mathrm{Im}\left(\sum_n \frac{\langle\Phi_0^{\theta}|\sum_j r_j e^{i\theta}|\Phi_n^{\theta}\rangle\langle\Phi_n^{\theta}|\sum_j r_j e^{i\theta}|\Phi_0^{\theta}\rangle}{E_n^{\theta} - E_0^{\theta} - \hbar\omega}\right), \tag{4}$$

where $|\Phi_n^{\theta}\rangle$ and $\langle\Phi_n^{\theta}|$ shall be understood as the right and left eigenvectors of the rotated atomic Hamiltonian H^{θ} with eigenvalue E_n^{θ}, cf. the discussion about the inner product around Eq. (3). The usual sum over discrete states and integral over continuum states is here replaced with the sum over the finite eigenstates of the matrix representation of H^{θ} discussed above. The eigenvalues E_n^{θ} are generally complex, leading to finite denominators. The eigenstates representing the ordinary unstructured continuum have large imaginary parts, thus the contribution from each such state is smooth and varies slowly with ω. The coherent sum over these states gives, then, a good representation of the background photo-absorption also with a very modest number of states [30,31]. Resonances, on the other hand, around which the cross section might change rapidly, are eigenstates of H^{θ}. They appear explicitly in the sum in Eq. (4), and their contributions are accurately accounted for. The case of the photoabsorption spectrum illustrates clearly the benefits provided by complex rotation; the explicit representation of the resonances and the good representation of the unstructured continuum with few states.

Consider now a general wave function that can be written as a superposition of eigenvectors of a rotated atomic Hamiltonian, H^{θ}. It may, in close analogy with Eq. (4), be analyzed through the population per energy interval, $dP/d\varepsilon$ [24,29],

$$\frac{dP}{d\epsilon} = \frac{1}{\pi}\mathrm{Im}\left(\sum_n \frac{\langle\Psi^{\theta}|\Phi_n^{\theta}\rangle\langle\Phi_n^{\theta}|\Psi^{\theta}\rangle}{E_n^{\theta} - \epsilon}\right), \tag{5}$$

where ϵ is the total energy. Above the ionization threshold $dP/d\varepsilon$ yields the energy distribution in the continuum, which equals the photoelectron spectrum when only one ionization-channel is open. Again $|\Phi_n^{\theta}\rangle$ and $\langle\Phi_n^{\theta}|$ shall be understood as the right and left eigenvectors of the rotated atomic Hamiltonian, H^{θ}, with eigenvalue E_n^{θ}. Similarly, while the right state vector, $|\Psi^{\theta}\rangle$, is a superposition of right eigenvectors of H^{θ} the left state vector, $\langle\Psi^{\theta}|$, is a superposition of left eigenvectors of the same Hamiltonian. However, there is, unfortunately, no simple way to get the latter from the knowledge of the former. This is the key point: In order to be able to extract information about the continuum part of the wave function it is necessary to find a convenient way to obtain this superposition of left eigenvectors. We will discuss this further in Sec. II D and outline a solution in Sec. III.

C. Time-dependent systems

To monitor a quantum system in the time domain, we need to address the time-dependent Schrödinger equation,

$$i\hbar\frac{\partial}{\partial t}\Psi(\mathbf{r},t) = H(\mathbf{r},t)\Psi(\mathbf{r},t), \tag{6}$$

where H and Ψ are the Hamiltonian and the wave function of the system, respectively. With uniform complex scaling, Eq. (6) is modified to

$$i\hbar\frac{\partial}{\partial t}\Psi^{\theta}(\mathbf{r},t) = H^{\theta}(\mathbf{r},t)\Psi^{\theta}(\mathbf{r},t), \tag{7}$$

with

$$\Psi^{\theta}(\mathbf{r},t) \equiv \Psi(\mathbf{r}e^{i\theta},t), \tag{8}$$

and H^{θ} defined earlier in Eq. (2). The physical situation we want to describe is an initially bound state that is exposed to a short electromagnetic pulse, thereby an electronic wave packet is generated, localized in space and time, that travel outward. The wave function Ψ can, thus, be assumed to be an analytical function of $\mathbf{r}$ and t and square integrable. Consequently, Ψ^{θ} will also be square integrable and, thus,

$$\lim_{|\mathbf{r}|\to\infty}\Psi^{\theta}(\mathbf{r},t) = 0, \tag{9}$$

for all finite values of t.

In the search for a *numerical* solution of Eq. (7), Ψ^θ is represented in a *finite* basis and, thus, the wave function is effectively confined in a sphere of characteristic radius R,

$$\Psi^\theta(\mathbf{r},t) = 0, \quad \text{for } |\mathbf{r}| \geqslant R. \tag{10}$$

From Eq. (9) it is clear that for large enough R this constraint will not affect the solution. The radius, R, required for an adequate description of a specific system, depends obviously on the time duration during which we want to follow the wave packet, but it depends also on the choice of θ. To see this, consider, for example, a superposition of spherical outgoing waves,

$$\Psi(\mathbf{r}) = \sum_n c_n e^{ik_n r} \leftrightarrow \Psi^\theta(\mathbf{r}) = \sum_n c_n e^{-k_n(\sin\theta - i\cos\theta)r}, \tag{11}$$

where $k_n > 0$. In Eq. (11), the scaled wave packet is suppressed due to the damping coefficients $k_n \sin\theta$. Moreover, since a larger k_n gives a larger suppression, the fastest components in the wave packet will be most affected. Effectively, this will lead to a delay of the scaled wave packet compared to the unscaled one.

We divide now the Hamiltonian into a time-independent part, H_0^θ, and a time-dependent part, H_I^θ,

$$H^\theta(\mathbf{r},t) = H_0^\theta(\mathbf{r}) + H_I^\theta(\mathbf{r},t), \tag{12}$$

and expand the wave function in the eigenstates of the former,

$$\Psi^\theta(\mathbf{r},t) = \sum_n c_n^\theta(t)\Phi_n^\theta(\mathbf{r}), \tag{13}$$

where

$$H_0^\theta(\mathbf{r})\Phi_n^\theta(\mathbf{r}) = E_n^\theta \Phi_n^\theta(\mathbf{r}). \tag{14}$$

H_I^θ will in the following describe the time-dependent interaction between the atom and the laser pulse. Note that the general eigenvectors of H_0^θ are fundamentally different from the corresponding eigenvectors, Φ_n, of the Hermitian H_0. Only a subset of the former can be obtained from the latter as

$$\Phi_b^\theta(\mathbf{r}) = \Phi_b(\mathbf{r}e^{i\theta}). \tag{15}$$

The subscript b indicates that the relation is indeed valid only for bound eigenstates or, more precisely, for states Φ_b decaying sufficiently fast when $r \to \infty$, where they are unaffected when confined to the part of space where $r < R$. The eigenenergy of any of these functions Φ_b^θ is then also real and identical to that of Φ_b. Of even more significance in the present context is that the corresponding coefficients c_b^θ in Eq. (13), are then θ independent. The nonbound eigenstates of H_0^θ have, on the other hand, complex eigenenergies [with $\mathrm{Im}(E_n^\theta) < 0$] and lack any simple connection to the eigenstates of H_0.

D. The left state vector

Assuming that the time-dependent Schrödniger equation has been solved and Ψ^θ has been found, we now set out to extract physical information from it. How can this be done? One obvious approach would be to transform the final Ψ^θ back to Ψ,

$$\Psi^\theta(\mathbf{r},t) \to \Psi(\mathbf{r},t), \tag{16}$$

$$\leftrightarrow$$

$$\sum_n c_n^\theta(t)\Phi_n^\theta(\mathbf{r}) \to \sum_n c_n(t)\Phi_n(\mathbf{r}), \tag{17}$$

where Φ_n^θ and Φ_n are the eigenstates of H_0^θ and H_0, respectively. Once Ψ is constructed we can proceed in the traditional manner. As discussed in connection to Eq. (15), the coefficients in Eq. (17) that are associated with bound eigenstates are θ independent. This particular part of Ψ is, thus, easily retrieved. For nonbound eigenstates there is, however, no simple way to find the expansion coefficients for the unrotated wave function from the knowledge of those of the rotated one. One alternative, that has been discussed, e.g., by Buchleitner *et al.* [32,33], is to perform a back-transformation through the application of the (back)-rotation operator

$$\Psi(\mathbf{r},t) = e^{\frac{i3\theta}{2}} e^{\frac{\theta}{2\hbar}(\mathbf{r}\cdot\mathbf{p}+\mathbf{p}\cdot\mathbf{r})}\Psi^\theta(\mathbf{r},t). \tag{18}$$

However, a brute-force application of Eq. (18) is, unfortunately, feasible only in very few cases. Since the amplitude of any outgoing wave component in Ψ^θ decays exponentially with r, cf. Eq. (11), the back-rotation operator has in some regions of space to recover Ψ from a heavily suppressed part of Ψ^θ. This is connected with truly large eigenvalues of the operator $(\mathbf{r}\cdot\mathbf{p} + \mathbf{p}\cdot\mathbf{r})$, and the application of the back-rotation operator quickly yields numerically very unstable results.

An alternative to the *active* transformation of Ψ^θ back to Ψ in Eq. (18), could be a *passive* transformation of the system, i.e., we keep Ψ^θ and transform the operators or functions that act on it. As has been discussed in Ref. [24], the expectation value of an operator $O(\mathbf{r})$ can be calculated with rotated wave functions as

$$\int \Psi^*(\mathbf{r},t)O(\mathbf{r})\Psi(\mathbf{r},t)dV = \int [\Psi^{-\theta}(\mathbf{r},t)]^* O^\theta(\mathbf{r})\Psi^\theta(\mathbf{r},t)e^{i3\theta}dV, \tag{19}$$

where $O^\theta(\mathbf{r}) \equiv O[\mathbf{r}\exp(i\theta)]$ and $[\Psi^{-\theta}(\mathbf{r},t)]^* \equiv \Psi^*[\mathbf{r}\exp(-i\theta),t]$. Hence, if both the left state vector, $(\Psi^{-\theta})^*$, and the right state vector, Ψ^θ, are known, all information about the system is accessible. Note, though, that Eq. (19) does not imply that the two integrands are equal. As in connection with Eq. (5) the final problem is how to construct the left state vector. Since it is as hard to retrieve $(\Psi^{-\theta})^*$ from Ψ^θ as it is to retrieve Ψ, we will, instead, set out to construct the left left state vector directly and in parallel with the construction of the right state vector.

E. The time evolution of the left and right state vector

While the right state vector is expanded in right eigenvectors of H_0^θ, Eq. (13), the left state vector will be a superposition of its left eigenvectors,

$$[\Psi^{-\theta}(\mathbf{r},t)]^* = \sum_n \left[c_n^{-\theta}(t)\right]^* \left[\Phi_n^{-\theta}(\mathbf{r})\right]^*. \tag{20}$$

As discussed in connection with Eq. (3), a left eigenvector of H_0^θ, with eigenenergy E_n^θ, is the complex conjugate of the

right eigenvector of $H_0^{-\theta} \equiv (H_0^{\theta})^{\dagger}$, with eigenenergy $E_n^{-\theta} = (E_n^{\theta})^*$. We now have to find the time-dependent c coefficients separately for the right and the left state vector.

The Schrödinger equation (7), can be recasted into an equation for the coefficients c_n^{θ} of the right state vector. Collecting the coefficients in Eq. (13) in a single vector $\mathbf{c}^{\theta}$, we have the following matrix equation:

$$i\hbar \frac{\partial}{\partial t}\mathbf{c}^{\theta}(t) = \left[\mathbf{H}_0^{\theta} + \mathbf{H}_I^{\theta}(t)\right]\mathbf{c}^{\theta}(t), \tag{21}$$

where the individual matrix elements of $\mathbf{H}_0$ and $\mathbf{H}_I$ are given by

$$\begin{aligned} \left[\mathbf{H}_0^{\theta}\right]_{nj} &= E_n^{\theta}\delta_{nj} \\ \left[\mathbf{H}_I^{\theta}(t)\right]_{nj} &= \int \left[\Phi_n^{-\theta}(\mathbf{r})\right]^* H_I^{\theta}(t)\Phi_j^{\theta}(\mathbf{r})e^{i3\theta}\,dV. \end{aligned} \tag{22}$$

Let us, first, consider the time evolution for a *time-independent* Hamiltonian. With $\mathbf{H}_I^{\theta}(t) \equiv 0$, the $\mathbf{c}^{\theta}$ vector at time $t + \Delta t$ is given by

$$\mathbf{c}^{\theta}(t + \Delta t) = e^{-\frac{i}{\hbar}\mathbf{H}_0^{\theta}\Delta t}\mathbf{c}_n^{\theta}(t). \tag{23}$$

Note that the coefficients c_n^{θ} assigned to nonbound eigenstates of H_0^{θ} will decay exponentially since $\mathrm{Im}(E_n^{\theta}) < 0$. This reduction of the outgoing part of the wave function is also in accordance with the decay of the outgoing wave when $r \to \infty$, cf. Eq. (11).

The equation corresponding to Eq. (21), but for the coefficients $(c_n^{-\theta})^*$ in Eq. (20), is obtained from the Schrödinger equation (7), with rotation $-\theta$. Noting, further, that for an originally Hermitian matrix, $\mathbf{H}$, $(\mathbf{H}^{-\theta})^* = (\mathbf{H}^{\theta})^T$, we can write

$$-i\hbar \frac{\partial}{\partial t}[\mathbf{c}^{-\theta}(t)]^* = \left[\mathbf{H}_0^{\theta} + \mathbf{H}_I^{\theta}(t)\right]^T[\mathbf{c}^{-\theta}(t)]^*, \tag{24}$$

and, again, for $\mathbf{H}_I^{\theta}(t) \equiv 0$,

$$[\mathbf{c}^{-\theta}(t + \Delta t)]^* = e^{\frac{i}{\hbar}\mathbf{H}_0^{\theta}\Delta t}\left[\mathbf{c}_n^{\theta}(t)\right]^*, \tag{25}$$

where we have used that the time-independent Hamiltonian $\mathbf{H}_0^{\theta}$ is complex symmetric. Now the complex energies, E_n^{θ}, that caused the coefficients, c_n^{θ}, associated with nonbound eigenstates to decay, introduce instead an exponentially *increasing* factor in the coefficients, $(c_n^{-\theta})^*$.

We find, thus, that the price paid for the decaying coefficients, c_n^{θ}, in the right state vector increases coefficients in the left state vector. Similarly, the outgoing wave, Eq. (11), vanishing when $r \to \infty$, is accompanied by an exponentially growing incoming wave. However, the calculation of physical quantities generally requires a combination of c_n^{θ} and $(c_n^{-\theta})^*$ coefficients. As an interesting example consider, again, the population per energy interval, $dP/d\varepsilon$ given in Eq. (5). After inserting Eqs. (13) and (20) into Eq. (5) we get

$$\frac{dP(t)}{d\epsilon} = \frac{1}{\pi}\mathrm{Im}\left[\sum_n \frac{P_n^{\theta}(t)}{E_n^{\theta} - \epsilon}\right], \tag{26}$$

where

$$P_n^{\theta}(t) \equiv \left[c_n^{-\theta}(t)\right]^* c_n^{\theta}(t). \tag{27}$$

The quantity P_n^{θ} is finite for all times, and for the time-independent situation, $\mathbf{H}_I^{\theta}(t) \equiv 0$, it is also preserved in time.

Let us now turn to the time-dependent situation, where different eigenstates of $\mathbf{H}_0^{\theta}$ are coupled to one another through $\mathbf{H}_I^{\theta}$. As for the time-independent case, the calculation of $dP/d\epsilon$ requires that both vectors, $\mathbf{c}^{\theta}$ and $(\mathbf{c}^{-\theta})^*$, are accurately known. Similar to the solution of the time-dependent Schrödinger equation without complex scaling, the challenge lies primarily in the coefficients associated with large eigenvalues. For Ψ^{θ}, as for the nonrotated wave function Ψ, the accuracy of the most energetic part might be difficult to guarantee, but the time evolution of the wave function is still usually stable. In other words, the error do not generally propagate to the rest of the wave function. For $(\Psi^{-\theta})^*$, the situation is much more serious. The exponential growth, caused by the complex E_n^{θ}-s, will here create instabilities in the integration scheme. For moderate time steps, the inadequate description of the energetic part of $(\Psi^{-\theta})^*$ will eventually ruin all other parts of the wave function as well. In practice, this means that the typical time step needed in any propagation scheme soon becomes too small for the calculation to be doable. In Sec. III we will suggest a complex path for the time propagation in order to remove these instabilities.

III. THE COMPLEX TIME PROPAGATION

A. Theory

We will now show that $(\Psi^{-\theta})^*$ is, indeed, possible to compute also for time-dependent systems; the trick is to continue the time variable, t, into the complex-valued plane. A similar trick will be seen to simplify the time evolution for Ψ^{θ} as well. Obviously, to extract physical information, we need eventually to bring the wave functions, Ψ^{θ} and $(\Psi^{-\theta})^*$, back to the real time axis. From Cauchy's theorem we know though that for Hamiltonians *holomorphic* (also known as analytic) in t, the wave functions we then obtain do not depend on the path of integration. Hence, a complex time propagation gives, in principle, the same result as a conventional propagation along the real time axis alone. The computational workload may, on the other hand, depend strongly on our choice of path. We wish, therefore, to use the knowledge of how a wave function behaves at complex times to find a propagation path, between the initial and some final time, along which the state vector is easy to compute.

Let us, first, discuss some of the known properties of wave functions at complex times and start with a *time-independent* Hermitian Hamiltonian, H_0. The wave function associated with such a Hamiltonian evolves in time according to

$$\Psi(\tilde{t}e^{i\alpha}) = e^{\frac{\sin\alpha}{\hbar}H_0\tilde{t}}e^{-\frac{i\cos\alpha}{\hbar}H_0\tilde{t}}\Psi(0), \tag{28}$$

where $t = \tilde{t}e^{i\alpha}$ and $\tilde{t}$ is real. Obviously, the L^2 norm of the above function is preserved only along the real time axis, where $\sin\alpha = 0$. For other directions in the complex time plane, $\sin\alpha \neq 0$ and the positive energy components of Ψ in Eq. (28) will decay $(-\pi < \alpha < 0)$ or grow $(0 < \alpha < \pi)$ exponentially with $\tilde{t}$. Since the decay rates increase with energy, an arbitrary initial wave packet, $\Psi(0)$, approaches the ground state of H_0 (after renormalization) as $\tilde{t} \to \infty$ when $-\pi < \alpha < 0$. We note in passing that this is the basis for an efficient way to obtain the ground state of a time-independent Hamiltonian, see, e.g., Refs. [34–36].

For a *complex scaled* but still time-independent Hamiltonian H_0^θ, the time evolution of the corresponding wave functions, Ψ^θ and $(\Psi^{-\theta})^*$, resemble formally that of Ψ in Eq. (28),

$$\Psi^\theta(\tilde{t}e^{i\alpha_\theta}) = e^{-\frac{i}{\hbar}H_0^\theta \tilde{t}e^{i\alpha_\theta}}\Psi^\theta(0), \tag{29}$$

$$[\Psi^{-\theta}(\tilde{t}e^{i\alpha_{-\theta}})]^* = e^{\frac{i}{\hbar}H_0^\theta \tilde{t}e^{-i\alpha_{-\theta}}}[\Psi^{-\theta}(0)]^*. \tag{30}$$

We put a subscript, $\pm\theta$, on α in Eqs. (29) and (30) to distinguish between the time evolution of Ψ^θ and $(\Psi^{-\theta})^*$. For the unbound energy spectrum of H_0^θ we have approximately $E^\theta = |E^\theta|\exp(-i2\theta)$. The components of Ψ^θ and $(\Psi^{-\theta})^*$ associated with these energies will then decay exponentially in time for $(2\theta - \pi) < \alpha_\theta < 2\theta$ and $-(2\theta + \pi) < \alpha_{-\theta} < -2\theta$, respectively. Note, next, that the product between the left and right state vector is preserved if $\alpha_\theta = -\alpha_{-\theta}$. This product will also be preserved for time-dependent systems, at least for Hamiltonians analytic in t, since $H^\theta[\tilde{t}\exp(i\alpha)] = [H^{-\theta}(\tilde{t}\exp(-i\alpha))]^\dagger$. Hence, following the discussion in connection to Eq. (3), the left eigenvectors of $H^\theta[\tilde{t}\exp(i\alpha)]$ equals the Hermitian conjugate of the right eigenvectors of $H^{-\theta}[\tilde{t}\exp(-i\alpha)]$. It is, however, not necessary to connect the right and left *state vector* at $t = \tilde{t}\exp(i\alpha)$ and $t = \tilde{t}\exp(-i\alpha)$, respectively; the two state vectors will instead be treated as independent functions in the complex time domain. This gives more flexibility.

Returning, finally, to *complex scaled and time-dependent* Hamiltonians, we set out to take advantage of the complex time-integration path to achieve a better control of the time evolution of the left, as well as the right, state vector. In principle, we have the possibility to chose an optimal path in the complex plane to enforce a suppression of the most energetic components of $(\Psi^{-\theta})^*$. To find this optimal path might in the general case, however, be rather complicated since the full Hamiltonian, $H^\theta(t) = H_0^\theta + H_1^\theta(t)$, now decides the paths in the complex time plane for which the unbound part of the wave function is suppressed. For situations where the H_0^θ part of H^θ dominates, the straight line path discussed above will, however, still be a reasonable choice. Note, though, that the critical constraint is the size of H_I^θ on the complex time path, where it might be much larger than along the real axis. For the right state vector, a propagation along the real time axis should generally be adequate, but we can do even better; complex time paths can be used to magnify the ionized part of Ψ^θ, and, hereby, the time evolution, also of this part of the wave function, will be easy to describe. We return to this in the next section.

B. A numerical example

We illustrate the idea of a complex time propagation for a hydrogen atom exposed to a single laser pulse. The different parts of the Hamiltonian in Eq. (12) read:

$$H_0^\theta = -\frac{\hbar^2\nabla^2}{2m}e^{-2i\theta} - \frac{e^2}{4\pi\epsilon_0 r}e^{-i\theta}, \tag{31}$$

$$H_1^\theta(t) = -i\hbar\frac{e}{m}A(t)e^{-i\theta}\nabla\cdot\hat{\mathbf{z}}. \tag{32}$$

In Eq. (32), the interaction between the electron and the linearly polarized laser pulse is given in the velocity gauge and in the dipole approximation, i.e., the spatial variations of the vector potential, $A\hat{\mathbf{z}}$, are neglected. We work with a Gaussian-shaped envelope of the laser pulse,

$$A(t)\hat{\mathbf{z}} = A_0 e^{-(t/T)^2}\sin(\omega t)\hat{\mathbf{z}}, \tag{33}$$

where T is connected to the duration of the pulse and ω is the angular frequency of the carrier wave. Specifically, we consider a pulse with $w = 0.6$ a.u. and $T = 4\pi/\omega \approx 21$ a.u. and a peak intensity of 1×10^{15} W/cm^2. Note that the Hamiltonian is, indeed, holomorphic in t, as required for propagation along a complex time path. The atom is prepared in the atomic ground state at $t \to -\infty$. To be able to compute the photoelectron spectrum at a time when the pulse can be said to be over, i.e., when $t \gg T$, we now seek the two state vectors at $t \to \infty$.

We expand the right and left state vectors in the left and right eigenvectors of H_0^θ, as seen in Eqs. (13) and (20), respectively. These eigenstates are, in turn, expanded in products of B splines [37] and spherical harmonics, Y_ℓ^m, i.e.,

$$\Psi^{\pm\theta}(\mathbf{r},t) = \sum_n c_n^{\pm\theta}(t)Y_{\ell(n)}^{m(n)}(\Omega)\sum_k \eta_{k,\ell}^{\pm\theta}\frac{B_k(r)}{r}, \tag{34}$$

where the $\eta_{k,\ell}^{\pm\theta}$s are obtained from a diagonalization of the H_0^θ matrix. The above expansions are well converged with $\ell_{\max} = 10$ and we use a set of seventh-order B splines defined on a linear knot sequence. If not stated otherwise, the distance between two consecutive knot points is 0.2 a.u. and the overall box size, R, is 200 a.u..

The initial (at $t \to -\infty$) left and right state vectors are, as discussed in connection to Eq. (17), easy to construct. These states are now to be propagated stepwise in time through applications of Eqs. (21) and (24), respectively. In the very first and last time step, a field-free propagation is assumed. In the first step, the initial state of the right, as well as the left, state vector is propagated from the real axis to a complex time coordinate. Since we know the expansion of the wave function in terms of eigenstates of H_0^θ, this introduces almost no numerical uncertainty. The same applies to the last step, where the wave function is brought back to the real time axis. The first and last step can be rather freely chosen. One has though to pay attention to the growth of the vector potential when one leaves the real axis. If it grows too much, a field free propagation will obviously not be accurate, even if the vector potential is very small on the real axis. Consider now the last time step, which propagates the wave function from a finite (complex) time, τ, to infinite real times,

$$\lim_{t\to\infty} c_n^\theta(t) = c_n^\theta(\tau^\theta)e^{-\frac{i}{\hbar}E_n^\theta(t-\tau^\theta)}, \tag{35}$$

$$\lim_{t\to\infty}\left[c_n^{-\theta}(t)\right]^* = \left[c_n^\theta(\tau^{-\theta})\right]^* e^{\frac{i}{\hbar}E_n^\theta[t-(\tau^{-\theta})^*]}. \tag{36}$$

Since this step involves only a trivial time evolution, we can easily compute the generalized population of the continuum

states in Eq. (27),

$$\lim_{t\to\infty} P_n^\theta(t) = c_n^\theta(\tau^\theta)\left[c_n^{-\theta}(\tau^{-\theta})\right]^* e^{\frac{i}{\hbar}E_n^\theta[\tau^\theta-(\tau^{-\theta})^*]}. \quad (37)$$

Once the pulse is over, this quantity is, indeed, preserved in time.

For the intermediate integration steps, where we account for the laser pulse, we use an exponential time differencing algorithm [38] based on a fourth-order Runge-Kutta method. It has been checked against an ordinary Runge-Kutta procedure within the interaction picture, i.e., an exponential Lawson scheme [39], and against the Krylov method [40]. All these propagation schemes do work, but for the field strength and complex rotation parameters considered, the method used here requires less computational work. It produces, e.g., reliable results with fewer time steps than the ordinary Runge-Kutta method.

Let us now discuss the choice of integration path for the intermediate time steps. For simplicity, we seek a straight line propagation path in the complex time plane along which the vector potential is of moderate size. The line is, therefore, chosen to intersect with the real axis at $t = 0$, i.e., close to the maximum of the vector potential. It is then given by $t = \tilde{t}\exp(i\alpha)$, where $\tilde{t}$ is real. Note also that for the vector potential in Eq. (33) $|\alpha|$ has to be $< \pi/4$, since it is necessary that

$$\lim_{\tilde{t}\to-\infty} A(\tilde{t}e^{i\alpha}) = 0. \quad (38)$$

if it should be possible to use a field-free propagation from the real axis to $t = \lim_{\tilde{t}\to-\infty}\tilde{t}\exp(i\alpha)$. To illustrate the difference between various integration paths, consider the approximate solution for photoabsorption in hydrogen based on first-order time-dependent perturbation theory,

$$c_n^\theta(\tilde{t}e^{i\alpha_\theta}) \propto e^{i\alpha_\theta}e^{-\frac{i}{\hbar}E_n^\theta\tilde{t}e^{i\alpha_\theta}} \times \int_{-\infty}^{\tilde{t}} A(\tilde{t}'e^{i\alpha_\theta})e^{-\frac{i}{\hbar}(E_0^\theta-E_n^\theta)\tilde{t}'e^{i\alpha_\theta}}d\tilde{t}', \quad (39)$$

$$\left[c_n^{-\theta}(\tilde{t}e^{i\alpha_{-\theta}})\right]^* \propto e^{-i\alpha_{-\theta}}e^{\frac{i}{\hbar}E_n^\theta\tilde{t}e^{-i\alpha_{-\theta}}} \times \int_{-\infty}^{\tilde{t}} A^*(\tilde{t}'e^{i\alpha_{-\theta}})e^{\frac{i}{\hbar}(E_0^\theta-E_n^\theta)\tilde{t}'e^{-i\alpha-\alpha}}d\tilde{t}', \quad (40)$$

where $n > 0$ and E_0^θ a.u. is the energy of the atomic ground state. Note that, since $|A(t)| = |A^*(-t^*)|$ for the vector potential in Eq. (33), the magnitude of the integrand in Eq. (39) at $t = \tilde{t}\exp(i\alpha_\theta)$ equals that of the integrand in Eq. (40) at $t = -\tilde{t}\exp(-i\alpha_{-\theta})$. With the assumption that the unbound eigenenergies can be written as $E_n^\theta = |E_n^\theta|\exp(-i2\theta)$ (which is approximately true), we show in Fig. 1 how the integrands in Eqs. (39) and (40) depend on $|E_n^\theta|$ and on α for the choice of $\theta = 5\pi/180$. In particular, we report the largest magnitude of the integrands along an infinitely long and straight line integration path defined by α as a function of $|E_n^\theta|$. The key point here is that large integrands implies large cancellations. Stable numerical results are obtained if such cancellations are minimized, which is achieved if the integrand is small over the entire integration path. In the two upper panels, two specific propagation paths are considered; one along the real time axis (left panel), i.e., $\alpha_{\pm\theta} = 0$, and one in the complex time plane (right panel) with $\alpha_\theta = 2\theta$, or, equivalently, $\alpha_{-\theta} = -2\theta$.

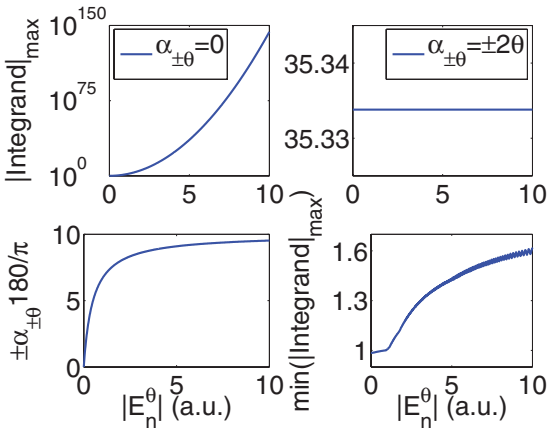

FIG. 1. (Color online) The maximum values of the integrands in Eqs. (39) and (40) seen along a straight line defined by α, given as a function of $|E_n^\theta|$, where $E_n^\theta = |E_n^\theta|\exp(-i2\theta)$, and calculated with $\theta = 5\pi/180$ a.u. and $E_0^\theta = -0.5$ a.u.. Due to symmetry reasons, the values presented for α_θ are identical to those of $-\alpha_{-\theta}$. The top left panel shows the peak integrand for a propagation along the real time axis. As E_n^θ increases, we see an exponential growth. The top right panel shows the same integrand but for an integration in the complex time plane. In particular, it shows the result with $\alpha_\theta = 2\theta$ or, equivalently, $\alpha_{-\theta} = -2\theta$. We see now that the magnitude of the integrand is independent of E_n^θ, since the complex parts of the time coordinate cancels that of E_n^θ. The bottom panels are generated by scanning through possible αs. In the right panel, we see the lowest upper bounds of the integrands and in the left panel are the corresponding values of α. The oscillations seen are due to a too-coarse scan.

Note the exponential growth as a function of $|E_n^\theta|$ of the former and the independence of $|E_n^\theta|$ in the latter. The $|E_n^\theta|$ independence along the complex path is related to the fact that $\mathrm{Im}[E_n^\theta\exp(\pm i\alpha_{\pm\theta})] = 0$ here, i.e., the imaginary parts in the two factors cancel each other. In the lower panels, we scan, instead, over different αs for each $|E_n^\theta|$. Note that the value of α (left panel), giving the smallest peak integrands in Eqs. (39) and (40) (right panel), varies with $|E_n^\theta|$. Even though not visible in the figure, the optimal αs in the left panel are given approximately by $\mathrm{Im}[(E_0^\theta - E_n^\theta)\exp(\pm i\alpha_{\pm\theta})] = 0$. This relation is expected for integration paths where A is relatively slowly varying. Overall, it is most important to control the magnitudes of the integrands that correspond to energetic components that otherwise might be very large. Hence, we should choose $\alpha_\theta \approx 2\theta$ and $\alpha_{-\theta} \approx -2\theta$, respectively. In Fig. 2, we now show a more detailed description of the integrands in Eqs. (39) and (40), respectively, for $|E_n^\theta| = 5$ a.u.. The symmetry between the two different integrands, when $\alpha_\theta = -\alpha_\theta$, is now clearly seen. Note also that the integration interval required for converged result depends on α. For Ψ^θ, the laser pulse stops, for instance, to contribute at an earlier stage in $\tilde{t}$ when $\alpha_\theta = 2\theta$ compared to $\alpha_\theta = 0$, but will, on the other hand, also start to contribute earlier. We can use these observations to optimize the integration path for Ψ^θ: a path along the real axis for $\tilde{t} \leqslant 0$ (black line) and in the complex plane ($\alpha \approx 2\theta$) for $\tilde{t} > 0$ (blue dashed line) gives a moderate-size integrand along the whole propagation path, as seen in the upper left panel of Fig. 2. For $(\Psi^{-\theta})^*$, a similar approach would, however, create

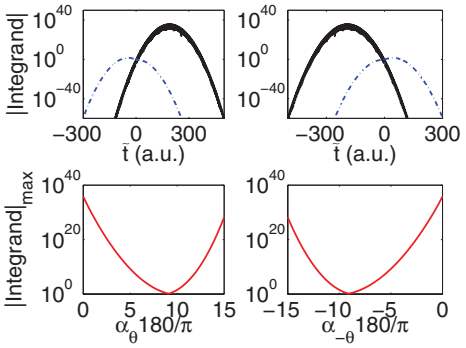

FIG. 2. (Color online) The left panels show the magnitude of the integrand in Eq. (39), whereas the right ones show the corresponding ones in Eq. (40). The given example is for $E_0^\theta = -0.5$ a.u. and $E_n^\theta = 5\exp(-i2\theta)$ a.u. with $\theta = 5\pi/180$. In the upper panels, the solid black lines are from an integration along the real time axis, i.e., $\alpha_{\pm\theta} = 0$, and the blue dashed lines from $\alpha_\theta = 2\theta$ and $\alpha_{-\theta} = -2\theta$, respectively. Even though not resolved, the integrands along the real time axis oscillate and vanish at certain times, i.e., when $\sin(\omega t) = 0$. As seen, the robustness of the numerical integration depends significantly on the chosen integration path.

instabilities in the integration scheme and cannot be used. To summarize, the wave functions are to be propagated along the lines

$$\Psi^\theta(\tilde{t}e^{i\alpha_\theta}) : \alpha_\theta = \begin{cases} 0, & \text{for } \tilde{t} \leqslant 0 \\ 2\theta - \gamma_\theta, & \text{otherwise} \end{cases}, \tag{41}$$

$$[\Psi^{-\theta}(\tilde{t}e^{i\alpha_{-\theta}})]^* : \alpha_{-\theta} = -2\theta - \gamma_{-\theta}, \tag{42}$$

where $\gamma_{\pm\theta} \geqslant 0$ are introduced as small constants to fine-tune the optimization of the integration schemes.

We are now finally in position to put the idea of a complex time propagation to a test. First and foremost, we need to verify that the integration paths extracted from first-order perturbation theory, Eqs. (41) and (42), are reasonable also for wave functions propagated stepwise in time. In the numerical calculation the laser pulse is accounted for from $\tilde{t} = -350$ a.u. to $\tilde{t} = 350$ a.u., and we use a constant time step, $\Delta\tilde{t}$, of 0.01 a.u. in this region of $\tilde{t}$. The time step is sufficiently small for a good representation of the time evolution and, on the other hand, large enough that the computing time is not an issue. We begin with the construction of $(\Psi^{-\theta})^*$. Figure 3 shows the population of the ground state computed from the left state vector and with different values of $\alpha_{-\theta}$. A scaling angle, θ, of $\pi/180$ is used and we include only energy components with $\mathrm{Re}(E_n^\theta) < 125$ a.u.. Note, first, that for large-enough magnitudes of $\alpha_{-\theta}$, we obtain α-independent results and, as anticipated from Eq. (40), the requirement is that $\alpha_{-\theta} < -2\theta$. For smaller magnitudes of α the results get increasingly unstable. Although the stable region can be increased if the time step is decreased, a calculation along the real time axis ($\alpha_{-\theta} = 0$) does not seem feasible for $(\Psi^{-\theta})^*$ even with the small value of θ used here.

Next, consider the right state vector Ψ^θ. From now on, all energy components of the wave functions are included. Here, we have chosen to propagate along the real time axis for $\tilde{t} \leqslant 0$, i.e., in agreement with Eq. (41), and consider the

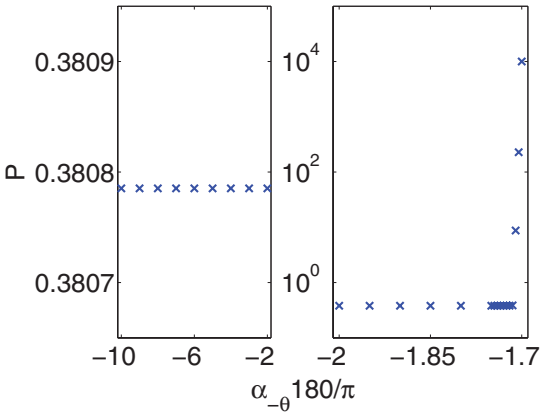

FIG. 3. (Color online) The population of the atomic ground state after exposure to the laser pulse. This population is here extracted from the *left* state vector $(\Psi^{-\theta})^*$, with $\theta = \pi/180$. Stable results are obtained when $\alpha_{-\theta} < -2\theta$.

possible choices for the remaining integration. Figure 4 shows the magnitudes of $c_n^\theta(t)\exp(iE_n^\theta t/\hbar)$, with c_n^θ in Eq. (13), for $\theta = 3\pi/180$ and for two different straight-line paths; one that continues along the real axis (red circles) and one in the complex plane (blue crosses). We have chosen the latter as in Eq. (41) with $\gamma_\theta = 0$. At the end of the integrations, i.e., at $t = 350$ a.u. and at $t = 350\exp(i2\theta)$ a.u., respectively, the two sets of $c_n^\theta(t)\exp(iE_n^\theta t/\hbar)$-s should be identical. The reason is that since $350 \gg T$, with T defined in Eq. (33), a field free propagation is reasonable from here onward. It is clear that the complex time path is able to produce numerically accurate values for much higher energy components of the wave functions than the one along the real time axis. In other words, the outgoing wave packet is easier to describe along a

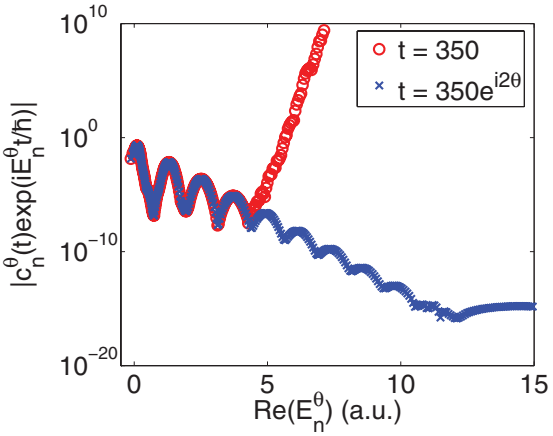

FIG. 4. (Color online) The magnitudes of $c_n^\theta(t)\exp(iE_n^\theta t/\hbar)$ for $\ell = 1$ and $\theta = 3\pi/180$, where c_n^θ are the expansion coefficients of the right state vector, Ψ^θ, in Eq. (13). These quantities are shown for a straight line integration from $t = 0$ a.u. to $t = 350$ a.u. (red circles) and to $t = 350\exp(i2\theta)$ a.u. (blue crosses). Since $350 \gg T$, where T is connected to the duration of the the considered laser pulse, the two sets of coefficients should be identical. As clearly seen, there is a numerical advantage of evaluating also the right state vector along a path in the complex time plane.

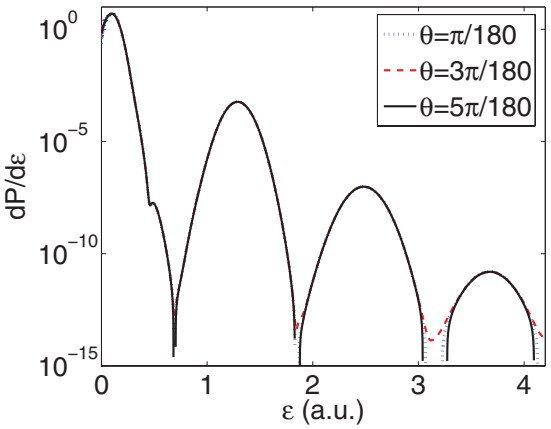

FIG. 5. (Color online) The photoelectron spectrum for the $\ell = 1$ angular symmetry computed as in Eq. (26). The four peaks corresponds to one, three, five, and seven photon absorption. Note the logarithmic y axis.

path in the complex time plane where it is neither enhanced nor suppressed in time.

The next step is to compute the photoelectron spectrum for different values of θ. As seen in Fig. 5, the results agree nicely for all considered cases, $\theta = \pi/180$, $3\pi/180$, and $5\pi/180$. The only deviation of some importance is found close to the ionization threshold. This part of the spectrum is seen in Fig. 6. Here, we note that the larger scaling angle (black line) seems to be favorable. This is because a larger scaling angle gives broader pseudocontinuum states in the real energy domain. Close to the threshold, this is particularly useful since an increase in the energy resolution otherwise requires a larger box for the calculation. Note that as $\theta \to 0$, the energy domain that is not welldescribed with this approach increases for a fixed box size.

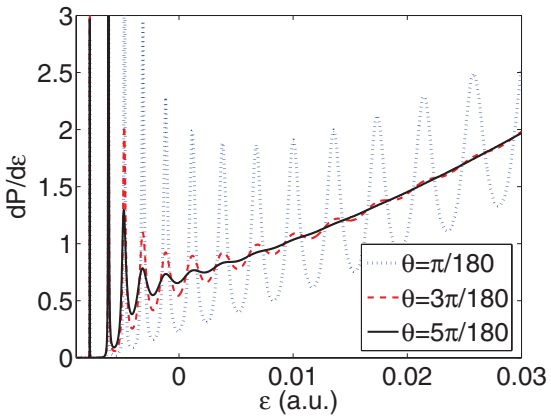

FIG. 6. (Color online) A close up on the photoelectron spectrum in Fig. 5. For the smallest scaling angle (dotted blue line), we clearly see the contribution to $dP/d\epsilon$ from the individual pseudocontinuum states. As θ increases, each such state gets a broader energy distribution that, eventually, will overlap with the neighboring states and the peaks in the spectrum vanishes. For the considered computational box, we are not able to adequately describe the Rydberg states below the ionization threshold. This explains why the threshold seems to be shifted downward in ϵ.

C. The choice of θ

Let us now briefly discuss the choice of scaling angle, θ. In all calculations with complex scaling one has to consider the variations in the results as a function of θ that arise due to numerical imperfections. For precision calculations of resonance parameters it is, in fact, not uncommon to look for an *optimal* value of θ, usually defined as the one that minimize the θ variations, see, e.g., Ref. [7]. One reason for the θ variation is the oscillations introduced in the wave functions when $r \to re^{i\theta}$ and which increase with increasing θ, thereby requiring an improved spatial representation for the same accuracy. Here we have seen that larger θ seems to give more stable results, see, e.g., Fig. 6, which we interpret as being due to the broader energy spread of the pseudocontinuum states. This broader spread gives an improved representation in the energy domain, which with a smaller θ can only be achieved with a denser pseudocontinuum spectrum. Still, for an optimal description of structures in the continuum, e.g., from multiphoton absorption, the spread should not be too broad. There is, thus, always a trade-off between different aspects when θ is chosen. When we now also chose a complex time path, additional aspects have to be considered. A larger θ requires an $\alpha_{-\theta}$ with larger magnitude to fulfill $\alpha_{-\theta} < -2\theta$. This brings the path further out in the complex plane, along which the vector potential in Eq. (33) might eventually grow to considerable size. The straight-line paths discussed above, and which is the best choice when H_0 dominates over H_I, might then have to be abandoned and one should probably consider an iterative approach to find a more appropriate integration path. A second consequence of a large θ is the earlier onset of artificial reflections from the box edge. Any analysis of the ionized part of the wave function has inevitably to be done before the electron wave packet reaches the outer boundary. The highest energy components of it will reach the boundary first, and even when they are not really of physical importance themselves, they will be reflected and then return to interfere with the more interesting components. For $(\Psi^{-\theta})^*$, this is a much bigger problem than for Ψ^{θ}. This is due to the increase of the coefficients, $(c_n^{-\theta})^*$ with t, cf. Eq. (25), which is more pronounced for larger θ. The coefficients, c_n^{θ}, of Ψ^{θ}, instead, decrease with t and the reflection is instead suppressed. Thus, the necessary box size differs for the two state vectors. This is illustrated in Fig. 7, where the population of the atomic ground state of hydrogen, after exposure to the laser pulse, is shown as a function of box size when calculated from the right (blue crosses) and the left (red circles) state functions, respectively. It is clear that the result is converged for much smaller box sizes for the right wave function. The scaling angle was here $\theta = 5\pi/180$ and the distance between two consecutive knot points in the B-spline basis was 0.5 a.u.. For larger rotation, the difference will be even more pronounced. It might still be possible, though, to improve the situation for $(\Psi^{-\theta})^*$ with the addition of a complex absorbing potential that can prevent the central part of the wave packet to be disturbed by reflected high-energy components. In summary, the optimal θ will then be one that is large enough for an accurate description of the continuum but small enough for $(\Psi^{-\theta})^*$ to fit inside the computational box. What this means in practice depends on the considered system.

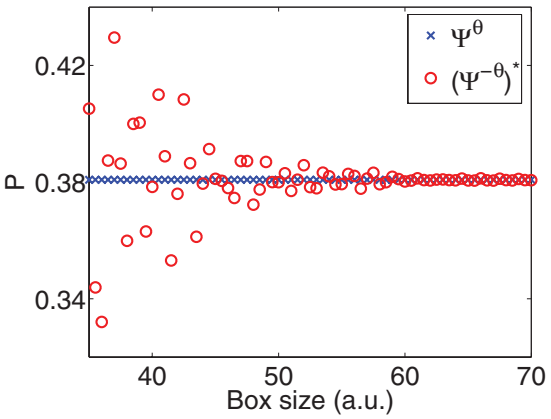

FIG. 7. (Color online) The population of the atomic ground state after the system has been exposed to the laser pulse in Eq. (33). The population is extracted from both the right (blue crosses) and the left state vector (red circles). Note that a larger box size is required when the population is extracted from $(\Psi^{-\theta})^{*}$.

IV. CONCLUSIONS AND OUTLOOK

The main purpose of this work was to demonstrate that information related directly to the continuum part of the wave function can rather easily be computed also with complex scaling. We need only to propagate the left and right state vector along a complex time path. Through this adjustment, one can, in a time-dependent calculation, take advantage of the usual benefits provided by complex scaling; the good continuum representation with rather few states due to their energy width and the possibility to represent resonant states. The latter has not been discussed in this work but will be the subject of a forthcoming paper. The drawback of the method is that the construction of the left state vector is rather cumbersome.

Although the use of a complex time path was primarily intended for the propagation of the left state vector, it proved to be useful also for the propagation of the right state vector. It might even be that a right state vector propagated along a complex path will be easier to rotate back to real r, cf. Eq. (17).

We have so far only studied the system after the pulse. To follow the dynamics also *during* the pulse one would need to make sure that the propagation path intersects with the real time axis at the point of interest. With the straight-line paths employed here a separate path should have to be used for each choice of t. This is, however, not a necessary procedure; it should be possible to adjust the path slightly in order to avoid recalculations from $t = -\infty$.

ACKNOWLEDGMENTS

Financial support from the Göran Gustafsson Foundation and the Swedish Research council (V.R.) is gratefully acknowledged.

[1] J. Aguilar and J. Combes, Commun. Math. Phys. **22**, 269 (1971).
[2] E. Balslev and J. Combes, Commun. Math. Phys. **22**, 280 (1971).
[3] B. Simon, Commun. Math. Phys. **27**, 1 (1972).
[4] B. Simon, Ann. Math. **97**, 247 (1973).
[5] G. D. Doolen, J. Nuttal, and R. W. Stagat, Phys. Rev. A **10**, 1612 (1974).
[6] Y. K. Ho, J. Phys. B **10**, L373 (1977).
[7] Y. K. Ho, J. Phys. B **12**, 387 (1979).
[8] K. T. Chung and B. F. Davis, Phys. Rev. A **26**, 3278 (1982).
[9] Y. K. Ho, Phys. Rev. A **48**, 3598 (1993).
[10] D. Wintgen and D. Delande, J. Phys. B **26**, L399 (1993).
[11] A. Bürgers, D. Wintgen, and J.-M. Rost, J. Phys. B **28**, 3163 (1995).
[12] E. Lindroth, Phys. Rev. A **49**, 4473 (1994).
[13] D. R. DeWitt, E. Lindroth, R. Schuch, H. Gao, T. Quinteros, and W. Zong, J. Phys. B **28**, L147 (1995).
[14] E. Lindroth and A.-M. Mårtensson-Pendrill, Phys. Rev. A **53**, 3151 (1996).
[15] S. Berkovic, R. Krivec, V. Mandelzweig, and L. Stotland, Phys. Rev. A **55**, 988 (1997).
[16] D. Nikolic and E. Lindroth, J. Phys. B **37**, L285 (2004).
[17] A. Maquet, Shih-I Chu, and W. P. Reinhardt, Phys. Rev. A **27**, 2946 (1983).
[18] A. Scrinzi, Phys. Rev. A **61**, 041402 (2000).
[19] I. A. Ivanov and Y. K. Ho, Phys. Rev. A **69**, 023407 (2004).
[20] J. H. Shirley, Phys. Rev. **138**, B979 (1965).
[21] S.-I. Chu and W. P. Reinhardt, Phys. Rev. Lett. **39**, 1195 (1977).
[22] C. R. Holt, M. G. Raymer, and W. P. Reinhardt, Phys. Rev. A **27**, 2971 (1983).
[23] A. Scrinzi and B. Piraux, Phys. Rev. A **58**, 1310 (1998).
[24] J. Bengtsson, E. Lindroth, and S. Selstø, Phys. Rev. A **78**, 032502 (2008).
[25] S. Selstø, E. Lindroth, and J. Bengtsson, Phys. Rev. A **79**, 043418 (2009).
[26] A. Csótó, B. Gyarmati, A. T. Kruppa, K. F. Pál, and N. Moiseyev, Phys. Rev. A **41**, 3469 (1990).
[27] R. Lefebvre, Phys. Rev. A **46**, 6071 (1992).
[28] N. Moiseyev, P. R. Certain, and F. Weinhold, Mol. Phys. **36**, 1613 (1978).
[29] T. N. Rescigno and V. McKoy, Phys. Rev. A **12**, 522 (1975).
[30] E. Lindroth, Phys. Rev. A **52**, 2737 (1995).
[31] J. L. Sanz-Vicario, E. Lindroth, and N. Brandefelt, Phys. Rev. A **66**, 052713 (2002).
[32] A. Buchleitner, B. Gremaud, and D. Delande, J. Phys. B **27**, 2663 (1994).
[33] A. Buchleitner, D. Delande, and J.-C. Gay, J. Opt. Soc. Am. B **12**, 505 (1995).
[34] A. D. Bandrauk, E. Dehghanian, and H. Lu, Chem. Phys. Lett. **419**, 346 (2006).
[35] S. A. Chin, S. Janecek, and E. Krotscheck, Chem. Phys. Lett. **470**, 342 (2009).
[36] L. Lehtovaara, J. Toivanen, and J. Eloranta, J. Comput. Phys. **221**, 148 (2007).
[37] C. deBoor, *A Practical Guide to Splines* (Springer-Verlag, New York, 1978).
[38] S. Krogstad, J. Comput. Phys. **203**, 72 (2005).
[39] J. D. Lawson, SIAM J. Numer. Anal. **4**, 372 (1967).
[40] E. S. Smyth, J. S. Parker, and K. T. Taylor, Comput. Phys. Commun. **114**, 1 (1998).